Provided for non-commercial research and education use.
Not for reproduction, distribution or commercial use.

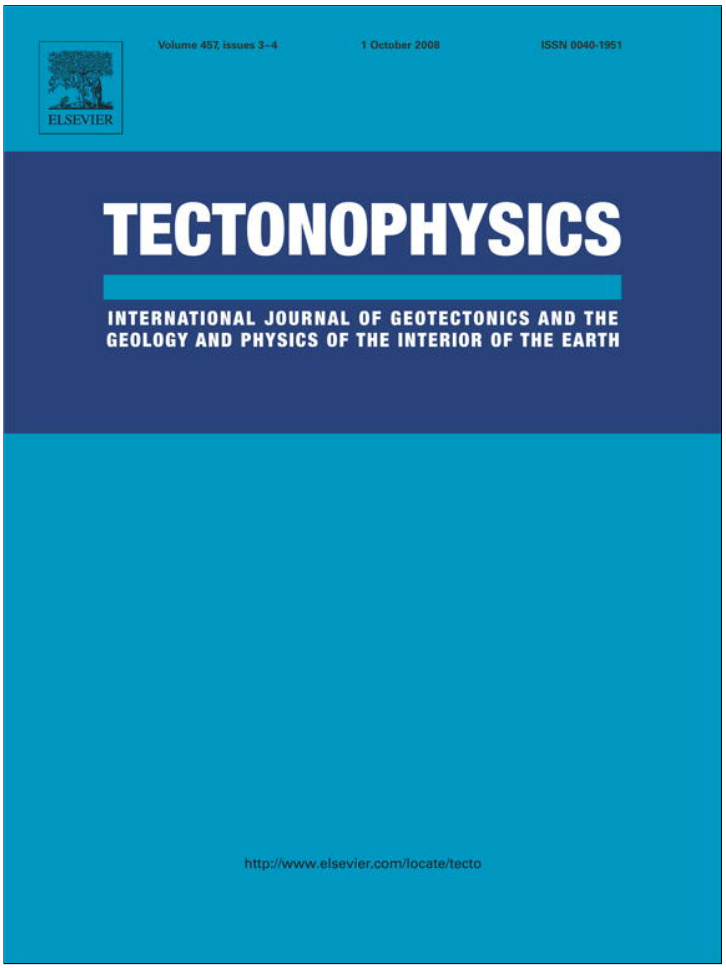

This article appeared in a journal published by Elsevier. The attached copy is furnished to the author for internal non-commercial research and education use, including for instruction at the authors institution and sharing with colleagues.

Other uses, including reproduction and distribution, or selling or licensing copies, or posting to personal, institutional or third party websites are prohibited.

In most cases authors are permitted to post their version of the article (e.g. in Word or Tex form) to their personal website or institutional repository. Authors requiring further information regarding Elsevier's archiving and manuscript policies are encouraged to visit:

http://www.elsevier.com/copyright

Author's personal copy

Tectonophysics 457 (2008) 209–223

Contents lists available at ScienceDirect

Tectonophysics

journal homepage: www.elsevier.com/locate/tecto

Vertical tectonic deformation associated with the San Andreas fault zone offshore of San Francisco, California

H.F. Ryan *, T. Parsons, R.W. Sliter

U.S. Geological Survey, Menlo Park, United States

ARTICLE INFO

Article history:
Received 30 January 2008
Received in revised form 3 June 2008
Accepted 5 June 2008
Available online 19 June 2008

Keywords:
Strike–slip fault
Finite element model
San Andreas fault
Merced Formation

ABSTRACT

A new fault map of the shelf offshore of San Francisco, California shows that faulting occurs as a distributed shear zone that involves many fault strands with the principal displacement taken up by the San Andreas fault and the eastern strand of the San Gregorio fault zone. Structures associated with the offshore faulting show compressive deformation near where the San Andreas fault goes offshore, but deformation becomes extensional several km to the north off of the Golden Gate. Our new fault map serves as the basis for a 3-D finite element model that shows that the block between the San Andreas and San Gregorio fault zone is subsiding at a long-term rate of about 0.2–0.3 mm/yr, with the maximum subsidence occurring northwest of the Golden Gate in the area of a mapped transtensional basin. Although the long-term rates of vertical displacement primarily show subsidence, the model of coseismic deformation associated with the 1906 San Francisco earthquake indicates that uplift on the order of 10–15 cm occurred in the block northeast of the San Andreas fault. Since 1906, 5–6 cm of regional subsidence has occurred in that block. One implication of our model is that the transfer of slip from the San Andreas fault to a fault 5 km to the east, the Golden Gate fault, is not required for the area offshore of San Francisco to be in extension. This has implications for both the deposition of thick Pliocene–Pleistocene sediments (the Merced Formation) observed east of the San Andreas fault, and the age of the Peninsula segment of the San Andreas fault.

Published by Elsevier B.V.

1. Introduction

Between one third and one half of the Earth's marine coastlines lie along or near tectonically active boundaries. Faulting can influence large-scale long-term changes in coastal geomorphology at millennial time scales by controlling changes in sediment supply and accommodation space. Although offsets along strike–slip fault zones are dominated by lateral motion, bends or step-overs can generate significant vertical displacements. Changes in fault geometry often correspond to changes in the geomorphic expression of the landscape (e.g. Zoback et al., 1999).

In this paper, we examine the implications of a strike–slip fault zone with non-parallel fault strands on the evolution of coastal geomorphology near San Francisco. For example, Ocean Beach in San Francisco, which is located 6 km north of where the San Andreas fault goes offshore, and is near the epicenter of the 1906 San Francisco Earthquake (Lomax, 2005; Fig. 1), has been subject to significant coastal erosion (Barnard et al., 2007). To determine the potential impact of active faulting on long-term coastal evolution near San Francisco, we updated the offshore fault map of Bruns et al. (2002) to identify changes in orientation and/or step-overs between adjacent fault strands. The revised digital representations of the faults are incorporated in a 3-D finite element model to examine the stress and strain implications of plate motion and fault slip. The model is used to determine rates of uplift and subsidence offshore of San Francisco. Both short-term vertical displacement such as coseismic deformation during the 1906 earthquake, and longer-term displacement resulting from many seismic cycles (repeat interval of 100's to 1000's of years) were calculated.

To validate calculated long-term vertical rates of deformation, we compare model results to coast-parallel elevation patterns of marine terraces (relative uplift) and the distribution of Holocene sediment on the Golden Gate platform (relative subsidence). Tide-gauge data combined with vertical elevation changes documented in the Lawson (1908) report were used to validate the coseismic displacement associated with the 1906 earthquake. We discuss the implications of the model for long-term fault step-over patterns on the Golden Gate platform, and suggest how the model could be improved to better match observations of vertical elevation changes during the Holocene.

2. Revised map of offshore faults

Our revised map of offshore faults was made from the interpretation of a combination of very high-resolution seismic reflection profiles (McCulloch, 1976; ten Brink and Driscoll, 1999), high-resolution multichannel seismic reflection (MCS) profiles (Childs

* Corresponding author. 345 Middlefield Rd. MS 999, Menlo Park, CA 94025, United States. Tel.: +1 650 329 5487.
E-mail address: hryan@usgs.gov (H.F. Ryan).

0040-1951/$ – see front matter. Published by Elsevier B.V.
doi:10.1016/j.tecto.2008.06.011

Author's personal copy

et al., 2000), and recently released industry deep penetration MCS profiles (USGS, 2006) (Fig. 2). These data were supplemented by 400 km of very high-resolution mini-sparker data that image reflectors up to 100 m sub-bottom acquired in September 2006 (Fig. 2).

Locations of the primary fault traces are similar to those shown by Bruns et al. (2002), with the major differences in interpretation related to the determination of recency of fault activity on individual fault traces. Recent faulting is generally indicated by offset of reflectors at or near the sea floor. However, it is particularly difficult to delineate offset of the sea floor beneath the Golden Gate platform, where very strong tidal currents near the Golden Gate have resulted in the deposition of a 10-m thick ebb-tide delta (Barnard et al., 2007; Fig. 1) that obscures recent faulting. In the vicinity of many of the fault strands, high-resolution mini-sparker data show abundant evidence of anomalous seismic reflection features that are typically attributed to the presence of gas, such as anomalous water-column reflectivity, sub-surface amplitude anomalies ("bright spots") and seismic data "wipeouts", which can mask recent fault activity. In addition, rough seas and a strong swell, characteristic of the platform area, can degrade the seismic signal, particularly in the shallow sub-bottom.

The primary fault traces mapped on the Golden Gate platform are: the Golden Gate fault, the San Andreas fault, the Potato Patch fault, and two main strands of the San Gregorio fault. Additional, less

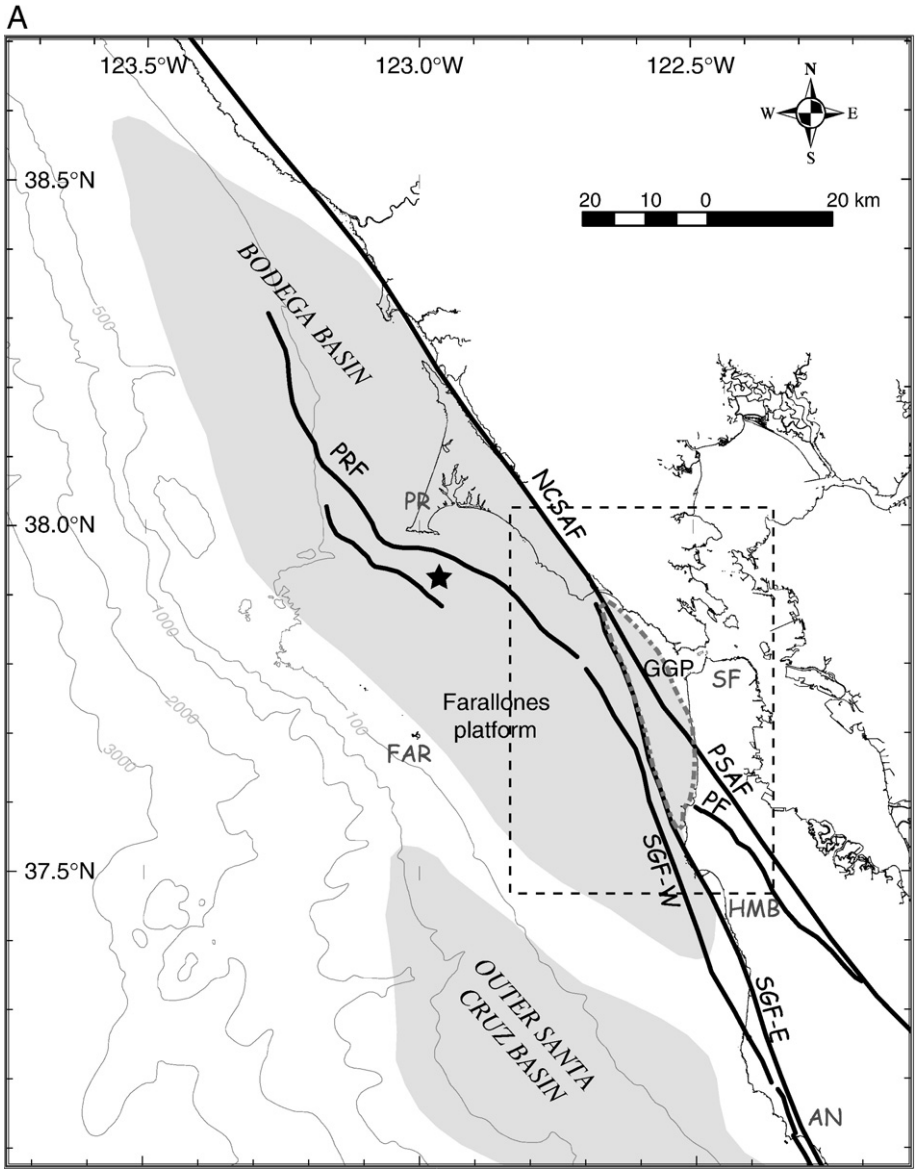

Fig. 1. A) Index map for B (dashed box) showing location of major faults (CGS, 2006 and this paper) and offshore basins (McCulloch, 1987); Bodega Basin has been modified from McCulloch, 1987 to extend further east. The location of the San Gregorio Basin of Bruns et al. (2002) is shown by gray dashed area east of the San Gregorio fault. Star denotes location of Shell offshore exploratory well 039-1ET. AN — Año Nuevo, FAR — Farallon Islands, GGP — Golden Gate platform, HMB — Half Moon Bay, NCSAF — North Coast San Andreas fault, PF — Pilarcitos fault, PR — Point Reyes, PRF — Point Reyes fault, PSAF — Peninsula San Andreas fault, SGF-E — San Gregorio fault-east, SGF-W — San Gregorio fault-west. B. Revised fault map for the offshore Golden Gate platform with additional faults from CGS (2006) (on shore SAF and SGF, PRF and PF), Kennedy (2002) (SF) and Galloway (1977) (WBF and EBF). Isopachs of inferred Holocene sediment deposited in the San Andreas graben are shown in blue with thickness in meters. Outcrop of Merced Formation is shown in yellow. Dashed gray line shows approximate location of the ebb-tide delta. Stars denote location of Great San Francisco Earthquake of 1906 (Lomax, 2005) and 1999 M5 earthquake off Bolinas (NCEDC, 2006). Gray lines show locations of seismic reflection profiles shown in this paper and gray hexagons show location of sections and seismic traces shown in Fig. 13. Bathymetric contour interval is 10 m (light blue lines). SCF — Seal Cove strand of San Gregorio Fault, SGF — San Gregorio fault, PPF — Potato Patch fault, SAF — San Andreas fault, GGF — Golden Gate fault, PRF — Point Reyes fault, WBF — western boundary fault, EBF — eastern boundary fault, PF — Pilarcitos fault, SF — Serra fault, B — Bolinas, FF — Fort Funston, FP — Fort Point, GG — Golden Gate, HMB — Half Moon Bay, LM — Lake Merced, MR — Mussel Rock, OB — Ocean Beach, PL — Point Lobos, SB — Stinson Beach.

Author's personal copy

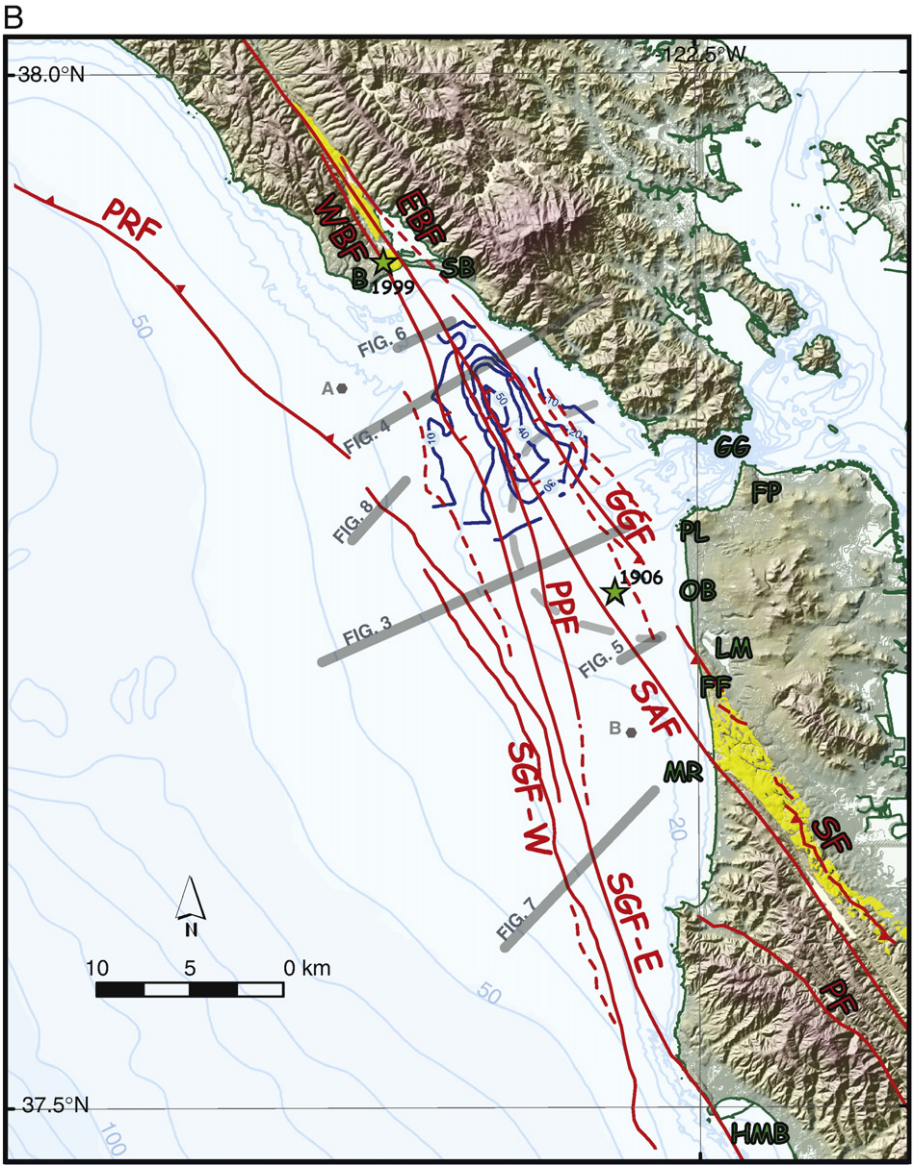

Fig. 1 (*continued*).

continuous fault strands were also mapped, particularly within the San Gregorio structural zone of Bruns et al. (2002). Below we discuss the major faults considered for input into the kinematic model: the Golden Gate, San Andreas, and San Gregorio fault zones. Since it is generally not possible to determine strike–slip displacement on seismic reflection profiles, it is assumed that all of these faults are primarily strike–slip faults, given the tectonic setting. Many of the faults also show vertical displacements and thus are oblique slip or form positive or negative flower structures. These differences in vertical displacement are important, however, in understanding fault interactions (Sylvester, 1976).

2.1. Golden Gate fault

The main strand of the Golden Gate fault zone lies 2–3 km northeast of the San Andreas fault and trends N35°W from offshore of Pt Lobos to southeast of Stinson Beach (Fig. 1). Only a few high-resolution MCS profiles cross this strand. Between Point Lobos and the Golden Gate, the fault generally shows normal separation with dips of about 55–70° to the southwest (e.g. Fig. 3); in other locations the fault is near vertical. The fault is best imaged north of the Golden Gate on very high-resolution profiles where it shows normal separation (Figs. 1 and 4). Here, the fault follows the eastern edge of a transtensional basin, the San Andreas graben of Cooper, 1973. Although the sediment within the San Andreas graben has not been directly dated, Cooper (1973) suggested that the sediment is less than 10,000 yr old based on assuming that the base of the basin is the Holocene transgressive surface. The marine transgressive surface has been dated at 7770 yr beneath Bolinas Lagoon (Berquist, 1978). In addition to the main strand of the Golden Gate fault zone, as many as 4 additional strands have been mapped both east and west of the San Andreas fault, although these strands are generally not as well-imaged (Fig. 1B). Reflection profiles crossing the Golden Gate fault strand south of the 1906 epicenter (Fig. 1B) show evidence for shortening (e.g. Fig. 5), whereas those to the north show evidence for extension.

Northwest of the San Andreas graben, the Golden Gate fault most likely continues on land to merge with the eastern boundary fault of the San Andreas fault zone (Fig. 1), which goes offshore near Stinson Beach (Galloway, 1977). Along the eastern edge of Bolinas Lagoon, this structure was termed a “graben fault” by Berquist (1978) based on the

Author's personal copy

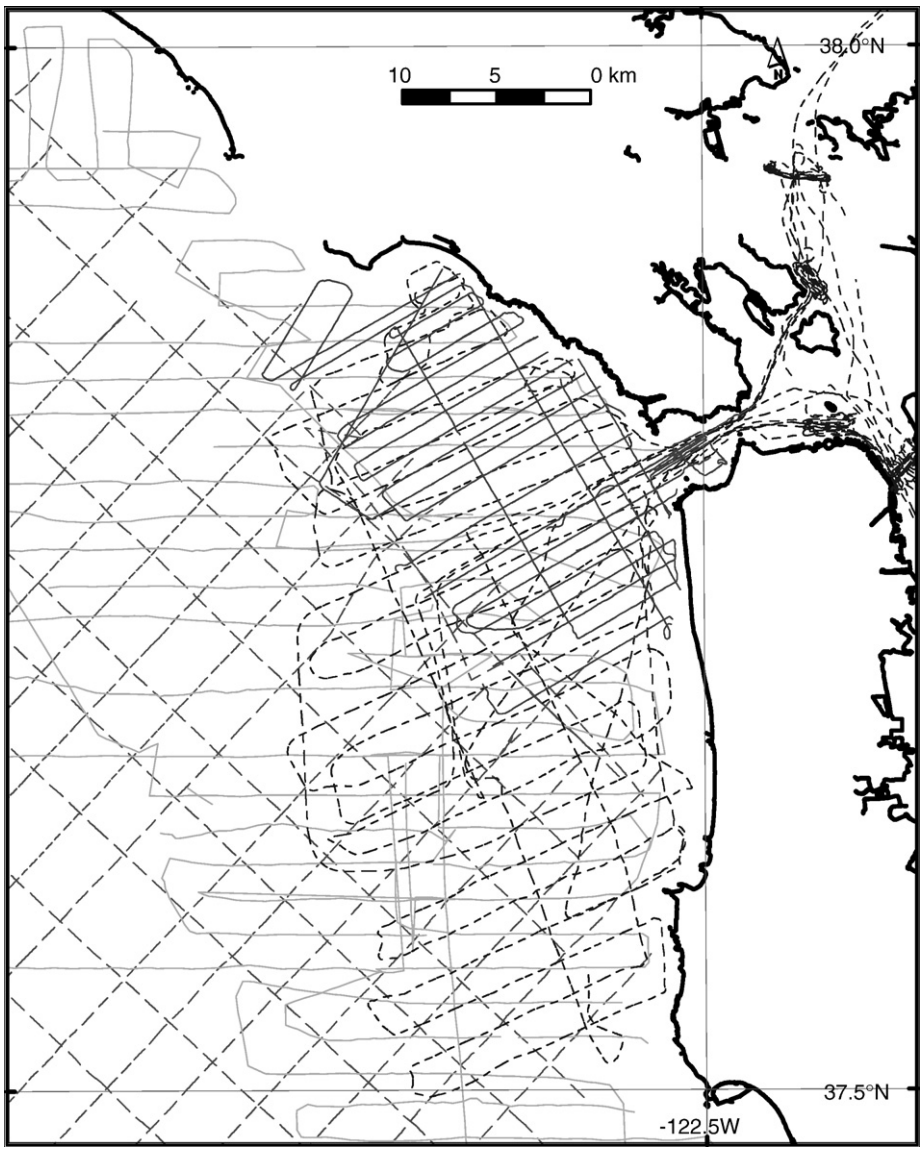

Fig. 2. Trackline map of seismic reflection profiles used to reinterpret offshore faults. Dashed lines are multichannel seismic reflection (MCS) lines with lighter dashes corresponding to industry MCS data (USGS, 2006) and darker dashes to high resolution MCS (Childs et al., 2000). Solid lines correspond to very high resolution profiles, with lighter lines corresponding to uniboom data collected in 1973 (McCulloch, 1976) and darker lines to recently acquired high resolution mini-sparker data.

interpretation of seismic reflection profiles. The eastern boundary fault, which is sub-parallel to and east of the main trace of San Andreas fault that ruptured in 1906, has pronounced topographic expression, although the fault "seems to disappear under terrace deposits to the northwest and southeast" (Galloway, 1977, p. 47). Grove and Niemi (2005) show that the eastern boundary fault trace truncates late Pleistocene sediment. South of the Golden Gate, the Golden Gate fault is more difficult to trace. It projects to the southeast toward Lake Merced (Fig. 1) in the vicinity of the Serra fault (Kennedy, 2002). The Serra fault is a blind thrust fault with evidence for Holocene displacement, which crosses the coast near Fort Funston (Kennedy, 2002).

2.2. San Andreas fault

The offshore section of the San Andreas fault extends from Mussel Rock, where the Peninsula segment of the San Andreas fault goes offshore, to the onshore North Coast segment of the San Andreas fault near Bolinas (Fig. 1; CGS, 2006). On land, the Peninsula segment of the San Andreas fault strikes at about N35°W and has a late Holocene slip rate of 17 mm/yr (Hall et al., 1999). Near Bolinas, the North Coast segment of the San Andreas fault also strikes at about N35°W (CGS, 2006) and lies within Quaternary deposits in the center of a valley between the western and eastern boundary faults (Galloway, 1977; Grove and Niemi, 2005). Paleoseismic studies reveal a late Holocene slip rate of 23 mm/yr on North Coast segment of the San Andreas fault, (Niemi and Hall, 1992); this slip rate is similar to slip rates calculated for the late Pleistocene and suggest that the rate has been constant over the last 30 ka and perhaps over the past 200–400 ka (Grove and Niemi, 2005).

The two land segments of the San Andreas fault do not line up along strike, but require a right releasing bend or step to join the two segments (Fig. 1). Northwest of Mussel Rock, the San Andreas fault continues offshore with a strike of N35°W for a distance of about 7 km. Along this section of the San Andreas fault, reflectors imaged northeast of the fault zone are folded and show evidence for compressive deformation (Fig. 4; ten Brink and Driscoll, 1999). The area of shortening occurs between the San Andreas fault and the offshore projection of the Serra fault (Kennedy, 2002). Northwest of the zone of compression, the offshore San Andreas fault makes a

Author's personal copy

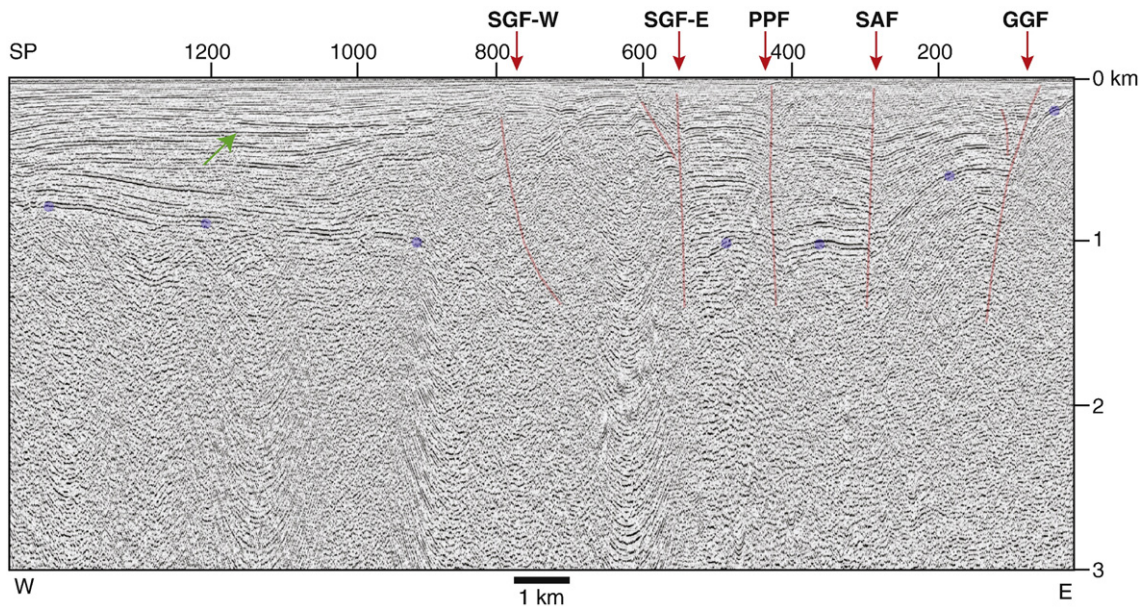

Fig. 3. Migrated and depth-converted high-resolution MCS profile showing principal offshore faults in Golden Gate platform (after Bruns et al., 2002). Velocity profile from Bruns et al. (2002) was used to depth convert the data. Blue dots show the approximate base of basins east and west of the San Gregorio fault zone (Horizons M1 and A of Bruns et al., 2002). West of the San Gregorio fault, reflectors can be tied to offshore exploratory well shown in Fig. 1A. The green arrow points at the reflector that corresponds to the approximate top of the Purisima Formation; the blue dots correspond to the top of the Monterey Formation. Vertical exaggeration is about 3:1. Location of profile is shown in Fig. 1B. (For interpretation of the references to colour in this figure legend, the reader is referred to the web version of this article.)

subtle change in orientation to about N30°W and maintains this strike until about 5 km southeast of where the fault goes onshore near Bolinas (Fig. 1). The fault cuts through the center of the San Andreas graben northwest of the Golden Gate (Fig. 1), and shows increasing down to the northeast vertical offset with subsurface depth (Fig. 5). Where the eastern San Gregorio fault converges with the San Andreas fault near Bolinas, the offshore San Andreas fault makes a slightly more westerly change in orientation to line up with the North Coast segment of the San Andreas fault, and reflectors between the two faults are shortened (Fig. 6).

2.3. San Gregorio fault

The San Gregorio fault lies primarily offshore and consists of two main fault strands beneath the Golden Gate platform: an eastern (Coastways) strand and a western (Frijoles) strand (Cooper, 1973; McCulloch, 1987), although Dickinson et al. (2005) consider the Frijoles strand to be a relatively minor fault. The area between these 2 strands is termed the San Gregorio structural zone by Bruns et al. (2002). The structural zone broadens to the north and is composed of multiple fault strands. The San Gregorio fault zone has a late Quaternary slip rate on

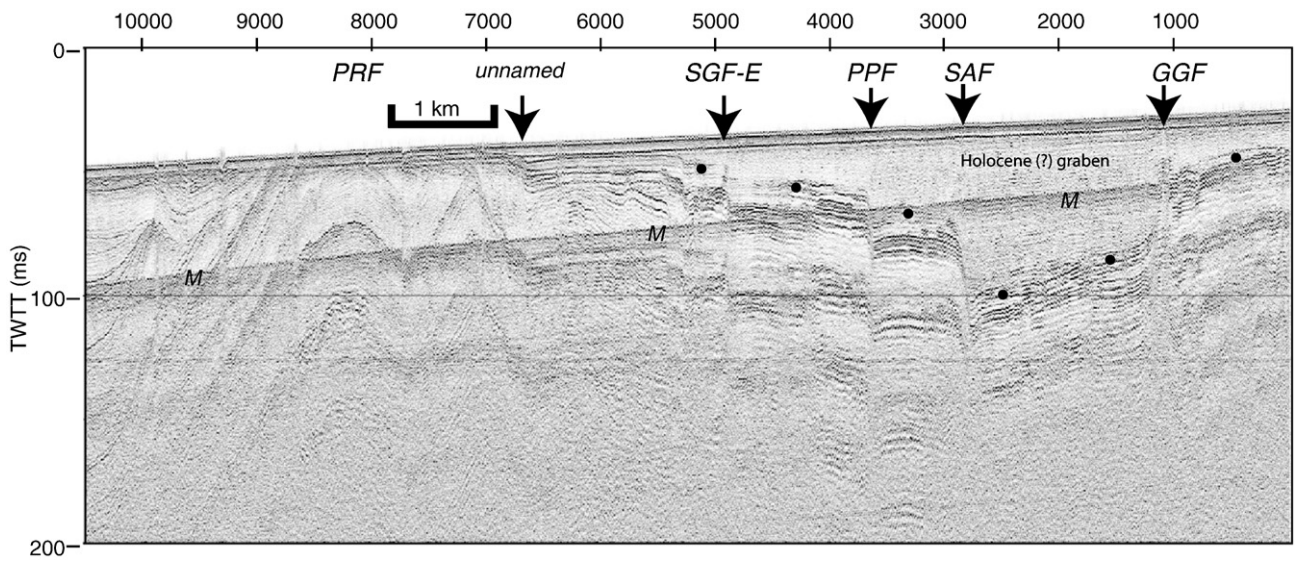

Fig. 4. Very high-resolution mini sparker profile across the San Andreas graben and Point Reyes fault zone. The maximum thickness of sediment in the inferred Holocene graben is on the order of 60 m. Note the narrow zone where deformation changes from extension associated with the graben to shortening associated with the Point Reyes fault zone to the west. Dots show base of graben; M denotes water bottom multiple. Vertical exaggeration is very high (about 30:1). TWTT — two-way travel time. Depth in m is approximate. Location of profile is shown in Fig. 1B.

Author's personal copy

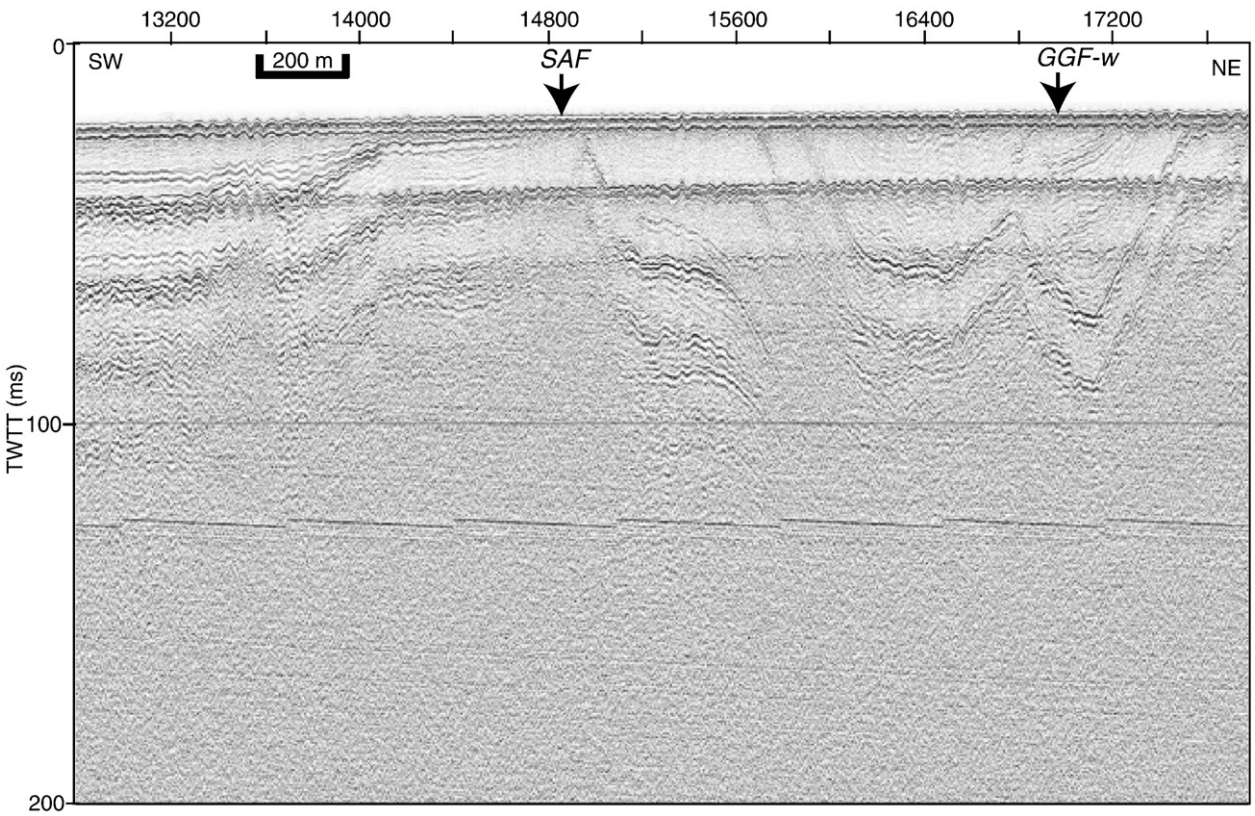

Fig. 5. Very high-resolution mini sparker profile across the San Andreas fault about 6 km northwest of where the fault goes offshore at Mussel Rock. Note that the fault deforms reflectors very near or at the sea floor. Reflectors are folded northeast of the fault and may be related to the offshore continuation of the Serra fault. Note that vertical exaggeration is high (about 10:1). TWTT — two-way travel time. Depth in m is approximate. Location of profile is shown in Fig. 1B.

the order of 7 mm/yr (WGCEP, 2003), although this rate was probably higher in the past (see Dickinson et al., 2005).

A strand of the San Gregorio fault is mapped on land as the Seal Cove fault near Half Moon Bay, where it strikes about N35°W and has a slip rate of about 4 mm/yr (Simpson et al., 1997). The Seal Cove fault is considered to be continuous with the main trace of the eastern San Gregorio fault mapped offshore (Bruns et al., 2002). North of Half Moon Bay, both strands of the San Gregorio fault zone bend to a more northerly orientation (N20°W) (Fig. 1). South of Mussel rock, industry MCS data clearly image both strands, which deform reflectors near the sea floor (Fig. 7). At depth, the western strand may dip to the east and merge with the eastern strand at depth (Fig. 7). Further north, the eastern strand of the San Gregorio fault forms the western edge of the San Andreas graben (Figs. 1 and 5). Near Bolinas, the eastern San Gregorio fault may merge with the western boundary fault of the San Andreas fault on land (Galloway, 1977; Grove and Niemi, 2005). Near the western boundary fault, a post-80 ka uplift rate of 1.0 mm/yr has been measured (Grove and Niemi, 2005). In 1999, a M5 earthquake with a thrust focal mechanism occurred near the southern end of the western boundary fault (Fig. 1, NCEDC, 2006).

The western strand of the San Gregorio fault is more difficult to map, particularly on very high-resolution reflection profiles, as the fault generally does not reach the sea floor. South of the latitude of Mussel Rock, the western strand has the same strike as the eastern strand (Fig. 1). However, the western strand diverges from the eastern strand to a more westerly orientation offshore of Fort Funston (Fig. 1). Where the western San Gregorio fault strikes more northwesterly, folding is more pronounced, particularly between the western San Gregorio fault and an unnamed fault strand to the east of it (Figs. 1 and 5). East of the area of shortening associated with the western San Gregorio fault, the eastern San Gregorio fault is in extension, with the distance separating the change from reverse to normal faulting being less than 1 km (Fig. 5). Slip on the western San Gregorio fault may merge with the Point Reyes fault zone further to the west.

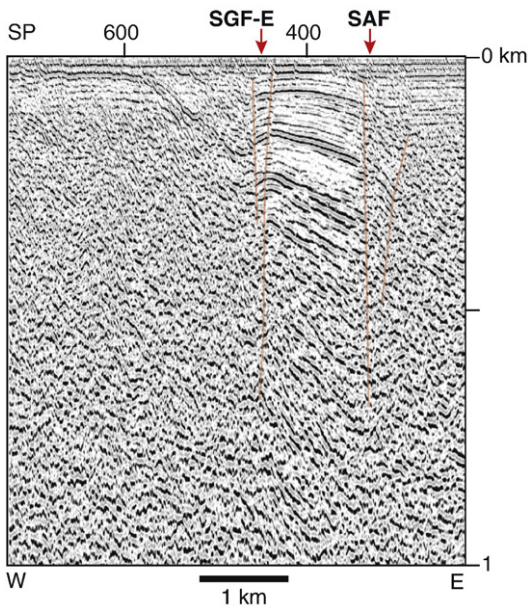

Fig. 6. Migrated and depth converted high-resolution MCS profile across SGF and SAF near where the faults converge southeast of Bolinas. Note that the reflectors are slightly shortened between the fault zones. Vertical exaggeration is about 6:1. Location of profile is shown in Fig. 1B.

Author's personal copy

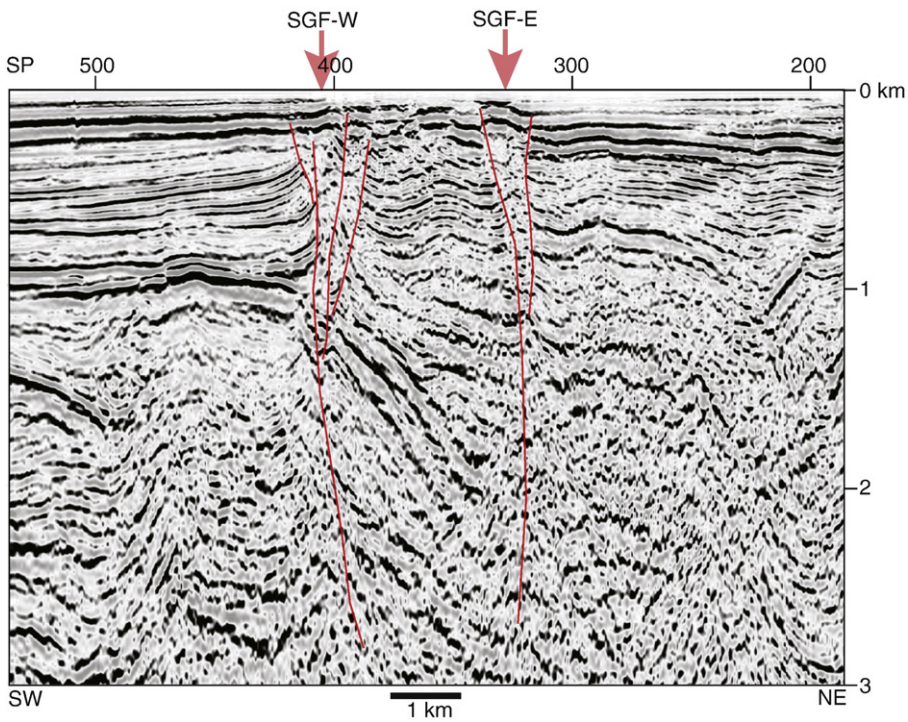

Fig. 7. Migrated and depth-converted industry MCS profile across main strands of the San Gregorio fault zone. Vertical exaggeration is about 3:1. Location of profile is shown in Fig. 1B.

2.4. Summary of revised fault map

No vertical sea floor offsets were observed across any of the fault strands that would substantiate recency of movement (e.g. see Fig. 5), however because movement is primarily strike–slip with little vertical displacement, strong tidal currents and the deposition of sediment in the ebb-tide delta is likely to have removed any evidence for vertical fault offset. Although no sea floor offset has been observed, near surface sediment is deformed on many of the reflection profiles. For example, the San Andreas fault clearly deforms sediment near or at the sea floor in the vicinity of where the fault goes offshore at both Mussel Rock and Bolinas (e.g. Figs. 4 and 6).

All fault strands (including the 1906 rupture) show evidence, locally, for burial as indicated by the imaging of reflectors beneath the seafloor that are undisturbed, although no systematic pattern related to the depth of fault burial appears to exist. The apparent burial, in some areas, may be an artifact of poor imaging of near-surface reflectors or the result of acoustic anomalies (gas?) that disturb or 'wipe-out' reflectivity. In the area of the San Andreas graben, faults appear to be buried by as much as 60 m of sediment (e.g. Fig. 5). However, Holocene shelf sediment typically is acoustically transparent and thus it is difficult to document fault offset. Although most of the faults are observed at the sea floor in places at least locally, the western strand of the San Gregorio fault zone is generally buried by sediment of probable Holocene age in the area west of the Golden Gate.

2.5. Step-over to the Golden Gate fault

Various lines of evidence, including below sea level topography, the presence of an inferred Holocene graben northwest of the Golden Gate (Cooper, 1973; Bruns et al., 2002), and the predominance of normal focal mechanisms in regional microseismicity (Zoback et al., 1999) indicate that the Golden Gate platform is under extension. Many models suggest that this extension is related to right stepping of fault slip to the Golden Gate fault from the San Andreas fault (Jachens and Zoback, 1999, Zoback et al., 1999; Wakabayashi et al., 2004), and that additional right stepping exists between the San Gregorio fault and the Golden Gate fault (Bruns et al., 2002). Evidence supporting the interpretation that most slip steps over to the Golden Gate fault includes a pronounced magnetic gradient across the Golden Gate fault, suggesting that it is a major boundary between rock bodies of differing magnetic susceptibility (Jachens and Zoback, 1999).

New information about fault structures, however, raises some important questions concerning details of the right-step model. If the principal San Andreas fault displacement zone is along the Golden Gate fault as suggested by Jachens and Zoback (1999), then a left step back to the North Coast segment of the San Andreas fault also must occur, which is inconsistent with the observed extensional basin in the left-step area. Some reflection profiles show that the Golden Gate fault dips into and thus probably intersects the San Andreas fault at relatively shallow, non-seismogenic depths. Faults that bound the extensional graben in the step-over zone are parallel to the main fault traces and not transverse as proposed by previous models developed to explain the formation of the basin between the San Andreas and Golden Gate faults (Bruns et al., 2002; Wakabayashi et al., 2004). Overall, the faults beneath the Golden Gate platform form a distributed shear zone with no evidence for progressive step-over in slip from west to east as indicated by the similar recency of faulting for most fault strands. All of the fault strands most likely accommodate some of the strike–slip motion, with no evidence suggesting that the Golden Gate fault, itself, is the principal plate-bounding fault. Therefore, we do not step all of the slip from either the San Gregorio fault or the San Andreas fault to the Golden Gate fault.

3. Kinematic model

3.1. Implications of fault geometry for coseismic, interseismic, and multicycle regional deformation

We identified several active faults in our remapping of the Golden Gate platform. However, an important question emerges; what are the long-term deformation implications if our fault model is correct, and do they match observed deformation? To investigate this issue, we conducted elastic-block modeling with blocks defined by the major

Author's personal copy

active faults in our map, and driven by observed geodetic velocities. A strike–slip fault that is perfectly aligned to regional tectonics would leave behind no observable strain around it. In an imperfectly aligned strike–slip system like the San Andreas, it is observations of vertical deformation that are especially diagnostic (e.g., Sylvester, 1976). In the system we have mapped on the Golden Gate platform, there are multiple active fault traces, steps, and junctions, which we expect to have produced vertical deformation. We thus compare model-derived changes in vertical elevation against observed patterns. We further explore shorter-term implications on vertical tectonics at different times in the seismic cycle.

We constructed a 3-D model of upper-crustal blocks using the finite element method following methods used by (Parsons, 2002, 2006a,b). The elastic part of the crust (upper 15 km) was simulated with 8-node, extruded brick elements (Fig. 8). The constitutive properties of the crust were approximated by those of wet Westerly granite and characterized by three elastic parameters: a Young's modulus of $E=8\cdot10^4$ MPa, a density of $\rho=2.7\cdot10^3$ kg m^{-3}, and a Poisson's ratio of $\sigma=0.25$. Elastic properties had very little impact on the results because the model was cut by through-going faults (Fig. 8); virtually any elastic constants would produce the same results because the elastic continuum is so much more difficult to deform than it is for faults to slip. The faults were deformable, and were constructed from contact elements that obeyed the Coulomb failure relation

$$\mathrm{CF}\equiv\overline{\tau}_f+\mu(\sigma_n) \tag{1}$$

where $\overline{\tau}_f$ was the shear stress acting on a fault surface, μ was the friction coefficient, and σ_n was the component of stress acting normal to a fault surface (pore fluid pressures were assumed constant and hydrostatic). Contact elements had zero thickness and were welded to the sides of the solid model elements. The modeled San Andreas fault passed through the model, defining two adjacent blocks. The western block was cut almost all the way through by the western San Gregorio fault, which terminated near the northwest model corner (Fig. 8). A minor strand of the San Gregorio fault zone, located between the east and west San Gregorio fault strands, was terminated within the western block as well.

The model free surface was unconstrained. The bottom of the model was free to move laterally, but not vertically, simulating an elastic layer overlying a less viscous substrate that, over the long term (many seismic cycles), builds no differential stress (Parsons et al., 2003). This assumption requires complete decoupling of vertical motions from the lower crust, which is unlikely in the real Earth; however, only small amounts of long-term vertical motions are expected relative to transform strain in the model. The advantages of this type of model are that the considerable uncertainties in representing the viscoelastic lower crust and upper mantle (e.g., Moresi et al., 2003; Muhlhaus and Regenauer-Lieb, 2005; Gerya and Yuen, 2007) do not factor into our results. The disadvantages are that our coseismic and interseismic results lack the transient signals associated with viscoelastic relaxation following large earthquakes, which for the Golden Gate platform region were shown to last about 36±16 yr after the 1906 earthquake by Kenner and Segall (2000). Our interests in this study, as well as the primary observational constraints, relate more to permanent deformation rather than transient.

All velocity constraints were imposed on the model edges; other than gravity, no constraints were imposed on elements within the model. Model blocks were displaced according to average velocities determined from Global Positioning System (GPS) observations (Fig. 8B). We held all elastic parameters fixed throughout the modeling, thus the only free parameter was the coefficient of friction on the faults, which could theoretically range from 0 to 1, though most investigators have concluded that the strike–slip faults of the San Andreas system have very low (μ=0.1–0.2) friction coefficients (e.g., Lachenbruch and Sass, 1980; Zoback, 1991; Reasenberg and Simpson, 1992; Bird and Kong, 1994; Miller, 1996; Parsons et al., 1999; Geist and Andrews, 2000).

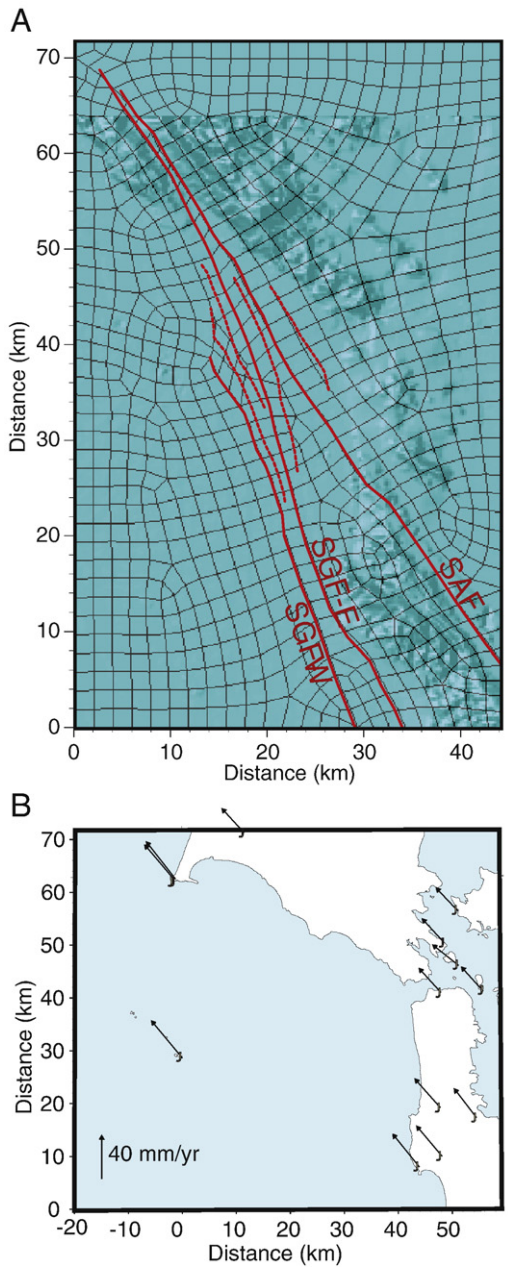

Fig. 8. (A) Finite element mesh. The 3-D model is 15 km thick. Each elastic element is approximately 2–3 km to a side. The model is cut by the faults shown as solid red lines. (B) GPS vectors used to displace the model blocks. SAF — San Andreas fault, SGF-E — San Gregorio fault-east, SGF-W — San Gregorio fault-west.

The finite element analysis was conducted using the ANSYS program. ANSYS employs the Newton–Raphson approach to solve nonlinear problems. In this method, a load is subdivided into a series of increments applied over several steps. Before each solution, the Newton–Raphson method evaluates the out-of-balance load vector, which is the difference between the restoring forces (the loads corresponding to the element stresses) and the applied loads. A linear solution is performed, using the out-of-balance loads, and checks for convergence. If convergence criteria are not satisfied, the out-of-balance load vector is re-evaluated, the stiffness matrix updated, and a new solution is obtained. The system of equations is solved through

Author's personal copy

direct elimination of equations until the problem converges (sparse direct solver).

3.2. Modeled multi-cycle deformation

Simulation of multiple earthquake cycles on the San Andreas and San Gregorio faults was accomplished by allowing model faults to slip continuously over a 20 kyr period, the assumption being that, over sufficient time, continuous slip produces the same deformation as repeated seismic slip episodes. Displacing model blocks according to GPS velocities caused variable slip on the San Andreas and San Gregorio faults, with San Andreas slip increasing northward from ~17 mm/yr to 22.5 mm/yr, and the San Gregorio slip decreasing northward from ~5 mm/yr to zero where it merges with the San Andreas fault (Fig. 9). Holocene geologic slip-rate estimates for the San Andreas fault are 17±4 mm/yr on San Francisco Peninsula and 24±3 mm/yr north of the Golden Gate; the north San Gregorio fault is estimated to slip at 7±3 mm/yr (Working Group on California Earthquake Probabilities (WGCEP), 2003). Thus modeled slip rates could replicate observed rates using a low friction coefficient of μ=0.1. The westernmost strand of the San Gregorio fault was included in the model, but it did not slip because the San Andreas and the longer San Gregorio strand took up all the displacement.

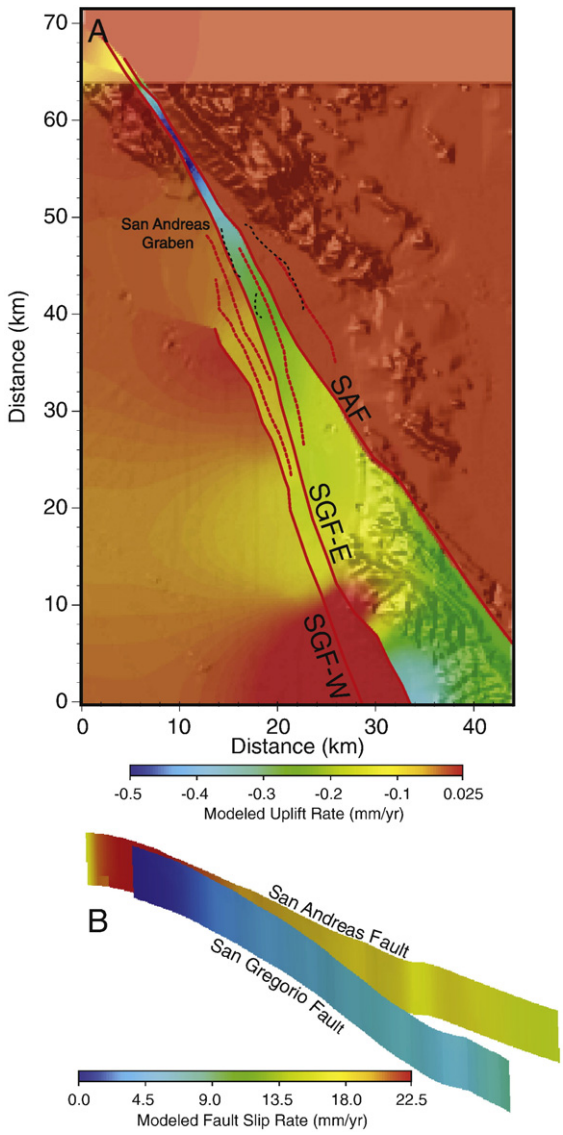

Fig. 9. (A) Long-term vertical deformation rates predicted by continuous slip on major strike–slip faults. Most of the region shows little vertical change except the block between the San Andreas and San Gregorio faults, which is predicted to subside as much as 0.5 mm/yr. (B) GPS-derived displacements replicated observed geologic slip rates on the San Gregorio and San Andreas faults. SAF — San Andreas fault, SGF-E — San Gregorio fault-east, SGF-W — San Gregorio fault-west.

Long-term slip on Golden Gate platform faults caused a very slight regional uplift of a maximum 0.025 mm/yr, which is effectively no vertical change. The exception in the model was the block between the San Gregorio and San Andreas faults, which was calculated to have subsided by a maximum 0.5 mm/yr (Fig. 9). The modeled area of maximum subsidence correlates spatially with the observed shallow Holocene basin on seismic profiles (Figs. 1 and 5). Subsidence occurred in the model because of the releasing orientation of the San Gregorio fault with respect to the relative motions of the crustal blocks determined from GPS observations. Broad extensional deformation in this region was inferred from normal-fault focal mechanisms on the Golden Gate platform by Zoback et al. (1999).

Our model predicts subsidence onshore between the San Gregorio and San Andreas faults to the south, where there now is relatively high topography (Fig. 9). We suggest that this high topography was originally compressed and uplifted by the restraining bend of the San Andreas fault in the vicinity of Loma Prieta. As the crust was transported northward, our modeling would imply that it began to subside in the releasing geometry between the San Gregorio and San Andreas faults, ultimately sinking below sea level.

3.3. Modeled coseismic deformation

We simulated coseismic deformation caused by the 1906 earthquake by displacing the San Andreas fault with the slip distribution of Thatcher et al. (1997). All other faults were locked and not allowed to slip. Prior to allowing the 1906 earthquake to occur in the model, we loaded the crust with 300 years (about the expected recurrence interval for 1906-type earthquakes (WGCEP, 2003) of interseismic strain. This was accomplished by locking all faults and straining the model according to GPS-derived displacements (Fig. 8B).

Modeled coseismic deformation associated with the 1906 earthquake is shown in Fig. 10. Broadly, areas to the northeast of the San Andreas fault were calculated to have been uplifted slightly (~0.1 m), while areas southwest of the fault were calculated to have subsided (as much as 0.6 m to the north). This deformation pattern is different than that of Geist and Zoback (1999), who calculated ~1 m of coseismic subsidence centered at the Golden Gate resulting from stepping the 1906 rupture across to the Golden Gate fault. Since the majority of the strike–slip motion was taken up by the San Andreas fault, we did not model 1906 strike slip on the Golden Gate fault. However, if the Golden Gate fault ruptured sympathetically with the 1906 earthquake, then our model could be reconciled with the Geist and Zoback (1999) calculations.

3.4. Post-1906 interseismic deformation

We simulated deformation over the hundred years elapsed since the 1906 earthquake by relocking the faults and moving the model blocks according to GPS-derived displacements. Our model indicates about 0.05 to 0.06 m of regional subsidence since 1906 (Fig. 10). Thus, in the model, about half of the calculated coseismic uplift east of the San Andreas fault has been erased by interseismic subsidence. The overall predicted pattern is one in which the entire Bay region subsides 0.1 to 0.2 m during San-Andreas-fault interseismic periods, and then areas east of the fault recover during 1906-type earthquakes. Offshore areas are predicted to subside both during and between San Andreas earthquakes. These predictions are largely consistent with topography, with stable areas lying above sea level, and areas of calculated subsidence lying offshore (Fig. 11). The exception is the Marin Headlands/Pt. Reyes Peninsula, which we calculated to be subsiding,

Author's personal copy

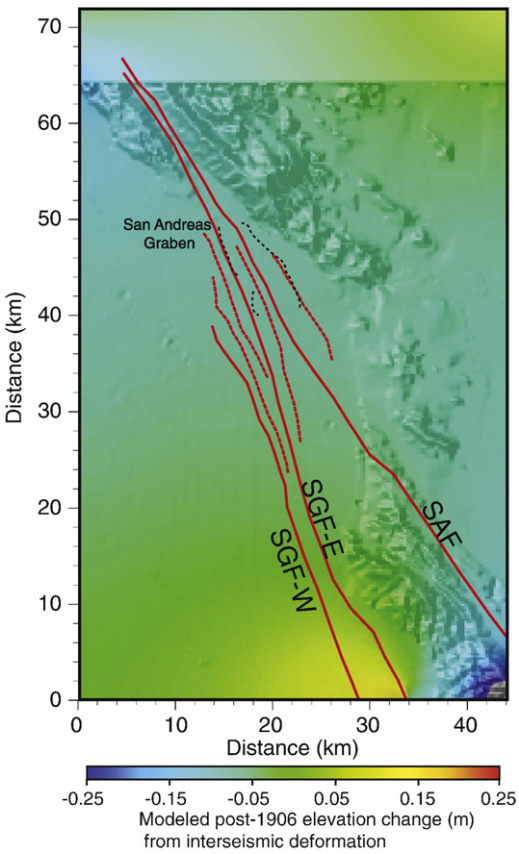

Fig. 10. Calculated post–1906 vertical interseismic deformation implies that about half of the coseismic uplift is erased in 100 years. Both post–seismic and coseismic deformation are calculated to cause subsidence offshore. SAF —– San Andreas fault, SGF–E —– San Gregorio fault–east, SGF–W —– San Gregorio fault–west.

but that lies well above sea level. This area may be influenced by thrust faults not included in the model (see section below).

4. Model implications

4.1. Regional deformation

As stated above, the finite element model does a reasonable job in predicting the first order topographic expression of the Golden Gate platform, which shows little predicted vertical elevation change related to faulting, except in the block between the San Gregorio and San Andreas faults. This block is predicted to subside at about 0.2 to 0.3 mm/yr. This is consistent with the 0.5 mm/yr subsidence determined from GPS and Interferometric Synthetic Aperture Radar (InSAR) data for the northern San Francisco Peninsula (Burgmann et al., 2006). However, locally, observed rates of Quaternary uplift and subsidence are greater than those predicted by the kinematic model.

The model predicts a maximum subsidence rate of 0.5 mm/yr for the area corresponding to the San Andreas graben, which is suggested to be Holocene in age (Cooper, 1973; Bruns et al., 2002) (Figs. 1 and 4). However, the maximum thickness of the basin is on the order of 60 m, which would require a subsidence rate of about an order of magnitude higher if the basin is Holocene in age. The basin is inferred to be Holocene based on the lack of reflectivity of basin sediment, which is characteristic of Holocene shallow water shelf deposits (Cooper, 1973). The assumption is made that the top of the reflective unit (shown by dots in Fig. 4) formed as a wave-cut platform during the previous low-stand in sea level and has since been deformed by faulting. The model's predicted rate of subsidence is similar to the 0.4 mm/yr Holocene subsidence rate determined for the 1906 trace of the San Andreas fault between Tomales Bay and Bolinas Lagoon (Grove and Niemi, 2005). At Bolinas Lagoon, Berquist (1978) measured around 1.7 mm/yr subsidence for early to middle Holocene deposits. The larger offshore subsidence as defined by the San Andreas graben suggests that either additional oblique slip motion on sub-parallel faults such as the Golden Gate fault may contribute to the higher subsidence rates, or that the base of the offshore basin is older than Holocene in age.

The model also does not predict areas of compressional uplift as documented by elevated Quaternary marine terraces both north and south of the Golden Gate. North of Mussel Rock, where the San Andreas fault goes offshore, late Pleistocene uplift rates of as high as 0.7–0.9 mm/yr have been measured at Thornton Beach based on the uplift of Olema-ash bearing deposits (55–75 ka) (Kennedy, 2002). The uplift at Thornton Beach may be related to movement on the Serra fault, which is not included in the model. The Serra fault is located 1.5 to 3 km northeast of the San Andreas fault, strikes N38°W, and dips 50°–60° to the southwest (Kennedy, 2002). Offshore reflection profiles show that the area between the San Andreas fault and an offshore continuation of the Serra fault is folded (Fig. 5; Cooper, 1973; ten Brink and Driscoll, 1999.) The Serra fault is part of a more extensive active east-vergent range front thrust system that has been mapped discontinuously for over 120 km to the southeast (McLaughlin et al., 1999); some of these thrust faults accommodated triggered slip and shortening during the Loma Prieta earthquake (Burgmann et al., 1997).

A major discrepancy between our model and observations is that the model predicts that the Marin Headlands/Pt. Reyes Peninsula is subsiding, but it lies well above sea level. This area may be influenced by reverse faults not included in the model. The Point Reyes Peninsula is uplifted by a high angle reverse fault, the Point Reyes fault, which was active during the Pleistocene (McCulloch, 1987; Grove, 2003). The San Gregorio and Point Reyes faults may at one time have been a single continuous fault sharing a common tectonic history (Dave McCulloch, pers. comm., 2006). Some of the slip from the western strand of the San Gregorio fault may be transferred to the Point Reyes fault, resulting in uplift of the peninsula.

4.2. Coseismic deformation

According to the Lawson (1908) report, "The general conclusion from both the leveling and the tidal observations is that, within the region examined, there occurred no general change in elevation to be detected with certainty." However the elevations of bench marks before and after the 1906 San Francisco earthquake show a general tendency for uplift at sites in the city of San Francisco (Lawson, 1908) as predicted by the finite element model.

NOAA (2001) acknowledges that a possibility exists for a small offset in the long-term relative sea level trends as measured at the tide gauge at Fort Point caused by the 1906 earthquake. We examined the tide-gauge record to determine whether the 10-cm signal associated with vertical uplift during the 1906 earthquake as predicted by our model is resolvable in the sea level signal. To attempt to isolate the tectonic signal from within the tide gauge data, we removed tidal fluctuations of less than 36 h using a low-pass filter, corrected the record for atmospheric pressure effects, and removed the annual cycle, which is dominated by temperature effects. Unfortunately, the residual signal in both the monthly-averaged and annual sea level data are still dominated by fluctuations of greater than 10 cm; these fluctuations are primarily related to climatic effects such as El Niño (Fig. 12; Ryan and Noble, 2002). In addition, as shown by the 19-year running mean, a change in the long-term rate of sea level rise associated with the end of the Little Ice Age in the mid to late 1800′s can also mask the 1906 co-seismic uplift.

As a way to test whether a 10-cm uplift is recorded in the tide-gauge record, we made the assumption that the slip did occur and

Author's personal copy

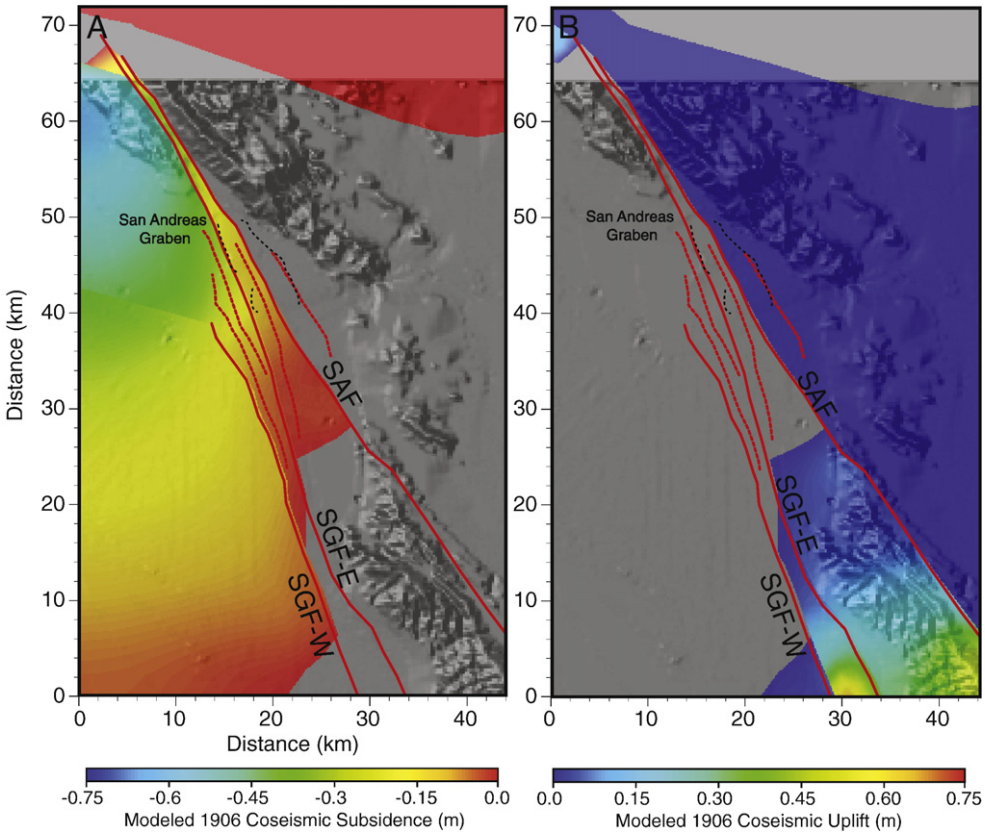

Fig. 11. Calculated vertical coseismic displacement associated with the 1906 earthquake. Subsidence (A) is shown separately from uplift (B). SAF — San Andreas fault, SGF-E — San Gregorio fault-east, SGF-W — San Gregorio fault-west.

removed the effect from the record. We then ran linear regressions on the rate of sea level rise for both the corrected and uncorrected data. The linear regression coefficient increased from 0.51 to 0.70 when we corrected for the 10-cm uplift. This suggests that the co-seismic uplift may be in the data, but not easily resolvable owing to the strong climatic overprinting.

4.3. Merced Formation and problem of strike–slip basin origin

One of the most compelling lines of evidence for a right step-over between the Golden Gate fault and the San Andreas fault is the interpretation that the Pliocene–Pleistocene Merced Formation accumulated in a narrow (<3 km wide) basin between the San Andreas fault and the San Bruno fault (which projects on land to the southeast of the Golden Gate fault). However, the results of our mapping and modeling indicate that the majority of slip on the San Andreas fault does not step over to the Golden Gate fault, which necessitates a reevaluation of the Merced Formation. In this section we present evidence that suggests that, in particular, the lower Merced Formation was not deposited in a simple pull-apart in a step-over zone.

The Merced Formation is a thick (1750 m) accumulation of shallow marine and coastal non-marine transgressive and regressive sequences deposited in an open ocean setting (Clifton and Hunter, 1987 and 1991; Clifton et al., 1988). Clifton and Hunter (1991) indicate that there is no stratigraphic evidence within the Merced Formation that faults were active during deposition or that it was deposited in a topographic trough. No fault scarp breccia has been observed along the basin boundaries, despite adequate exposures (Wakabayashi et al., 2004). A further indication that the Merced Formation was not deposited in a releasing step-over between 2 faults is that the formation is present in the subsurface over large areas north and east of where the Merced Formation crops out (e.g. Rogge and LaForce, 2002). In the offshore, thick (>1 km) basin sediment is not confined to a step-over zone, but occurs to the south and west of Mussel Rock, where the San Andreas fault goes offshore (e.g. Fig. 7).

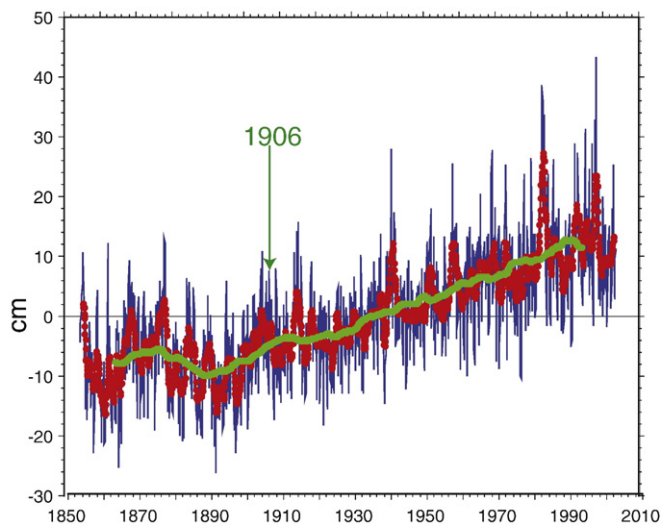

Fig. 12. Monthly mean tide-gauge data from Fort Point from 1858 to 2002 is shown in blue; 13-month running mean of monthly sea level is shown in red; 19-year running mean of monthly sea level is shown in green. The arrow points to April 1906. (For interpretation of the references to colour in this figure legend, the reader is referred to the web version of this article.)

Author's personal copy

Merced Formation sediment was deposited almost continually from late Pliocene to Pleistocene time, although the formation is not well dated (Clifton et al., 1988). The primary age controls are from within the upper 300 m of the Merced Formation where the Rockland ash bed was dated at 400–450 ka (Sarna-Wojcicki et al., 1985), but may be 100 ka older (Lanphere et al., 1999; Sarna-Wojcici, 2000). Changes in mineralogy from a Franciscan to Sierran source that occurred at about 600 ka provide an additional age control (Sarna-Wojcicki et al., 1985). Ingram and Ingle (1998) used the strontium isotopic composition of foraminifers to date the Merced Formation. They determined that only ages less than 1.2 Ma are well constrained (the upper 700 m of the section) and that the age of the oldest Merced Formation deposits is between 2.4 and 4.3 Ma (Ingram and Ingle, 1998).

The lack of evidence for faulting during deposition of much of the Merced Formation (Clifton and Hunter, 1991) combined with the possibility that the Merced Formation may be as old as 4 myr (Ingram and Ingle, 1998) suggests that at least the older Merced Formation was deposited prior to initiation of the Peninsula segment of the San Andreas fault. We explore the possibility that the older Merced Formation was initially deposited as a shoreline facies of a broader, large-scale basin that has since been dismembered and isolated structurally from the rest of the basin by strike–slip faulting, and subsequently uplifted by reverse faulting.

West of the San Gregorio fault zone, much of the Farallon platform is underlain by Bodega Basin (Fig. 1A, McCulloch, 1987). Bodega Basin is a large (180 by 25 km) predominately Neogene basin that extends from Half Moon Bay to Gualala (Fig. 1A). It contains over 3 km of late Miocene through Quaternary strata deposited on top of a late Miocene unconformity (McCulloch, 1987). An upper unit of Bodega Basin, the Purisima Formation, ranges in age from 7 to 2.58 myr (Powell et al., 2007). Younger, shallow-water facies of the Purisima Formation are present east of the main strand of the San Gregorio fault near Half Moon Bay (Powell et al., 2007) and are time correlative with the older Merced Formation deposits. We suggest that the oldest Merced Formation beds are shoreline deposits that accumulated along the landward edge of Bodega Basin and are time correlative with the youngest shallow marine Purisima Formation deposits.

In order to test this idea, we first compare the acoustic stratigraphy of Bodega basin to San Gregorio basin, which lies between the San Gregorio and Golden Gate faults (Fig. 1a, Bruns et al., 2002). Cooper (1973) first noted that reflectors east of the San Gregorio fault beneath the Golden Gate platform are acoustically similar to reflectors observed in Bodega Basin west of the fault zone. High-resolution MCS profiles image prominent reflectors near the base of Bodega basin (west of the faulting), and near the base of San Gregorio basin, between the San Gregorio and San Andreas faults (Horizons A and M1 of Bruns et al., 2002; delineated by blue dots in Fig. 3). Not only are the depths to the basins similar, but distinctive reflection packages can be visually correlated both east and west of the broad San Gregorio fault zone on most of the MCS profiles, even though significant horizontal displacement across the fault zone has occurred. Qualitatively, the stratigraphy across the faults is not substantially different as might be expected if one of the basins was formed in an extensional step over zone (i.e., San Gregorio basin) and the other was not (i.e., Bodega basin).

Various techniques were used to quantitatively correlate the stratigraphy on either side of the San Gregorio fault zone. The most effective technique involved the creation of a stratigraphic wave train by the vertical stacking of 10 adjacent multichannel seismic reflection traces that had been amplitude balanced with a full trace AGC (automatic gain control) applied. We created two vertically stacked wavelets that are located east and west of the San Gregorio fault zone, but offset about 23 km in a right-lateral sense (the maximum offset permitted based on good basin reflectivity on both sides of the fault — see Fig. 1b for locations) (Fig. 13). Lagged correlations were then calculated between the wavelets, which allowed for a vertical offset

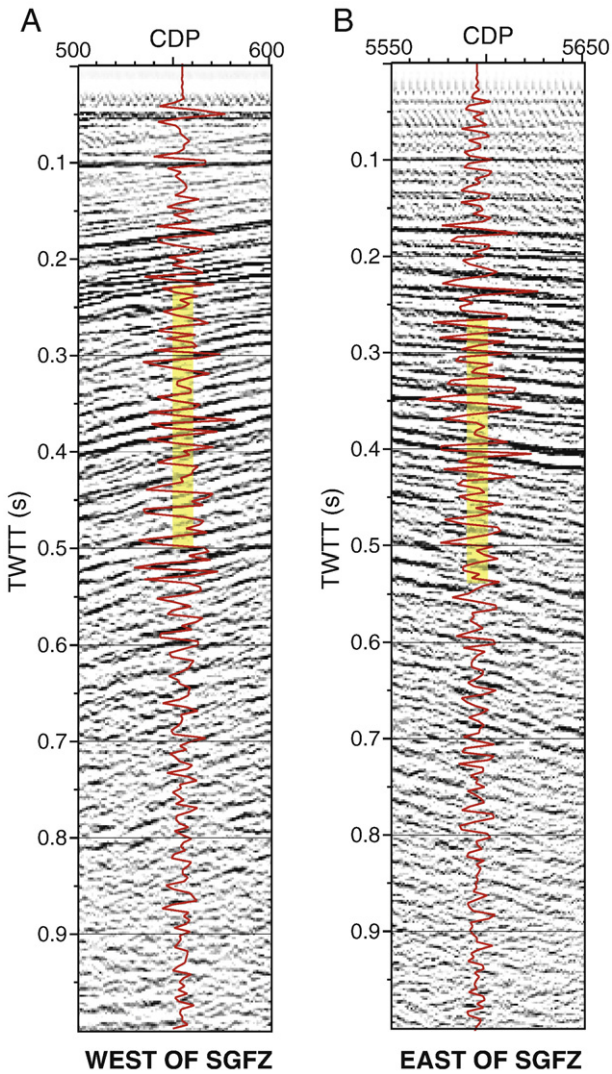

Fig. 13. High-resolution MCS profiles used to correlate across-fault stratigraphy. Section A is located west of the San Gregorio fault zone and 24 km northwest of section B, which is located east of the fault zone (locations are shown by hexagons in Fig. 1). The vertically-stacked wiggle traces are shown in red with the maximum lagged correlations occurring over the TWTT range shown in yellow. (For interpretation of the references to colour in this figure legend, the reader is referred to the web version of this article.)

between wavelets across the fault zone, with each lag corresponding to a 4 ms two-way travel time (TWTT) offset. Once the trace offset was determined, we systematically adjusted the start and end time of the wavelets until the correlation coefficient was maximized.

For the wavelets determined from the sections shown in Fig. 13, the maximum correlation was 0.49 for the TWTT interval of 220–500 ms (70 points in the wavelet). In order to determine if this correlation is significant at the 95% confidence limit for linear regression, we first determined the number of independent data points (N) by finding the zero-crossing of the autocorrelation for each wavelet and dividing the total number of data points by the zero-crossing. This yielded a total of 23 independent data points.

Using the following equation (Bendat and Piersol, 1986), we determined that any correlation above 0.41 is significant at the 95% confidence level.

95% confidence limit for correlation

$$= \left(e^{(2*1.96/\mathrm{sqrt}(N-3))}-1\right)\left(e^{(2*1.96/sqrt(N-3))}+1\right)^{-1}$$

Author's personal copy

Although a correlation of 0.49 is only slightly above the 95% confidence level, the fact that the wavelets are correlated at all allows for the possibility (but does not prove) that the stratigraphy is similar. We also tested wavelets over areas where no clear stratigraphic match was recognized and these tests yielded no correlations significant at the 95% confidence level (correlations were generally less than 0.2).

East of the San Gregorio fault zone, the top of the wavelet corresponds to a depth of about 240 m, which indicates that strata deposited below this depth are correlative with strata deposited in Bodega Basin. If the strata east of the San Gregorio fault are also correlative with the Merced Formation as suggested by Bruns et al. (2002), then this implies that part of the Merced Formation should also be correlative with Bodega basin strata. It should be pointed out, though, that no direct ties between the onshore and the offshore stratigraphy exist.

4.4. Peninsula San Andreas fault

Geodetic studies show that present motion between the Pacific plate and the Sierran microplate is oriented about N30°W and consists of right lateral simple shear with little evidence for contraction across the Bay Area (Savage et al., 2004; d'Alessio et al., 2005). Many faults, however, are not oriented along the optimal strike to accommodate this plate motion. On land, southeast of Mussel Rock, the Peninsula San Andreas fault strikes about N35°W, which is 5° counter–clockwise from present-day plate motions. The San Andreas fault continues along this strike for about 6–7 km offshore, but then changes strike to N30°W, in alignment with present plate motion. The Serra blind thrust (Kennedy, 2002) is active along the San Andreas fault where it is oriented in a more westerly direction (Fig. 1B), with the thrust fault not mapped further north of where the San Andreas changes orientation. Thus the Serra fault may be accommodating fault-perpendicular convergence owing to the more westerly fault orientation of the Peninsula segment of the San Andreas fault.

We explore the possibility of geologic control for the change in orientation of the San Andreas fault offshore of Mussel Rock. Jachens and Zoback (1999) show that a prominent magnetic anomaly associated with the Permanente terrane extends offshore for 6–7 km. The Permanente terrane is a distinctive belt of Franciscan Complex rocks of Cretaceous age that, on the San Francisco Peninsula, form a block between the Pilarcitos and San Andreas faults (McLaughlin et al., 1996). Parsons and Zoback (1997) provide evidence that the Permanente terrane is a deep-seated, high velocity body with densities greater than the surrounding Salinian and other Franciscan terranes. We suggest that the change in orientation of the San Andreas fault occurs near the northern termination of the Permanente terrane. The presence of a strong block may confine the location of the Peninsula segment of the San Andreas fault along its northwest boundary.

North of the Permanente terrane, the San Andreas fault is not constrained. Since slip is driven by the San Gregorio fault as it bends eastward to merge with the San Andreas fault, the slip on faults to the east (including the San Andreas fault) collapses into multiple strands accommodating both normal and strike–slip offsets. The easternmost of these strands lies near the edge of Bodega Basin (Fig. 1A and B), which may provide space for fault collapse. The proposed northern end of the Permanente terrane corresponds to the transition zone between fault-parallel shortening and extension, close to the epicenter of the 1906 earthquake. The northward migration of the Permanente terrane along the San Andreas fault may have contributed to the observed northwestward transgression of faulting along the range front thrust system (McLaughlin et al., 1999).

The offset of distinctive magnetic anomalies within the Permanente terrane across the Peninsula segment of the San Andreas fault constrains total right-lateral offset to 22 km (Jachens and Zoback, 1999). At the present slip rate of about 17 mm/yr (Hall et al., 1999), the Peninsula segment of the San Andreas fault would have initiated about 1.3 Ma. However, evidence is accumulating that long-term slip rates can be highly variable temporally with fault dynamics constantly changing through time as demonstrated by the East Bay fault system (Graymer et al., 2002). McLaughlin et al. (1996) suggest that from 8 to 6 Ma, Pacific–North American plate motion was primarily accommodated by slip on the East Bay fault system (including the Hayward, Calaveras and other faults), with much of the slip taken up by the Pilarcitos fault prior to this time. The timing of when some of this slip was transferred to the Peninsula segment of the San Andreas fault is unclear. Since the Pliocene, plate motions have been relatively constant (Atwater and Stock, 1998), and thus the initiation of the Peninsula segment of the San Andreas fault cannot be tied directly to changes in plate motion. A young age for the Peninsula San Andreas fault is supported by the lack of syntectonic deformation in much of the Merced Formation. Offshore, nearly two thirds of the strata imaged on reflection profiles between the San Gregorio and Golden Gate faults were deposited before the San Andreas fault became active (Bruns et al., 2002). In addition, McLaughlin et al. (2007) present new long term displacement data from the Pilarcitos fault and Peninsula segment of the San Andreas fault to show that the Peninsula San Andreas fault was initiated as late as 1.0–1.6 Ma. This young age is consistent with our observations based on the offshore stratigraphy.

5. Conclusions

We have interpreted a new fault map of the offshore Golden Gate platform between Half Moon Bay and Bolinas, California. The San Gregorio, San Andreas, and Golden Gate faults do not show a progressive step-over from west to east, but rather form a distributed shear zone across the Golden Gate platform. A kinematic model calculated for a 10,000-yr time span using the new fault geometries shows little vertical motion associated with faulting, except in the block between the San Gregorio and San Andreas faults, which is subsiding. Thus extension on the Golden Gate platform can be explained by the junction between the San Gregorio and San Andreas faults and does not require a right bend or step between the faults. Additional faults such as the Point Reyes fault and the Serra fault need to be incorporated in the model to account for localized uplift. In addition to determining multicycle deformation, coseismic uplift for a single earthquake event, the 1906 San Francisco earthquake, was calculated to be on the order of 10–15 cm, however, interseismic deformation has recovered about 5–6 cm of this uplift since 1906.

An important implication of the new fault model is that the bulk of the Merced Formation was not deposited within a step-over basin between the San Andreas and Golden Gate faults. Rather, we suggest that the lower Merced Formation was deposited as part of a large regional offshore basin, the Bodega basin, and then was subsequently dismembered by the San Andreas fault and uplifted by the Serra fault. This requires that the initiation of the Peninsula segment of the San Andreas fault post-dates lower Merced Formation deposition. The Serra thrust fault is thought to accommodate compression across the Peninsula segment of the San Andreas fault, which is oriented more westerly than present plate motions as indicated by geodetic studies. The more westerly orientation of the Peninsula segment of the San Andreas fault may be constrained by the deep-seated, resistant Permanente terrane.

Acknowledgments

We would like to dedicate this paper to Terry Bruns, whose initial interpretations of faulting off the Golden Gate formed the basis for this study. Sadly, Terry passed away in September 2006. We thank Bob McLaughlin and Dave Scholl for early reviews of this manuscript. In particular, we would like to thank Chris Sorlien for his thorough review, which improved the manuscript. Taras Gerya and an anonymous reviewer helped us to clarify the ideas in this paper.

Author's personal copy

References

d'Alessio, M.A., Johanson, I.A., Burgmann, R., 2005. Slicing up the San Francisco Bay area: Block kinematics and fault slip rates from GPS-derived surface velocities. Journal of Geophysical Research 110, B06403. doi:10.1029/2004JB003496.

Atwater, T., Stock, J., 1998. Pacific–North America plate tectonics of the Neogene southwestern United States: an update. International Geology Review 40, 375–402.

Barnard, P. L., Eshleman, J., Erikson, L., and Hanes, D. M., 2007. Coastal processes study at Ocean Beach, San Francisco, CA: Summary of data collection 2004–2006. U. S. Geological Survey Open-file Report. 2007–1217, 165 pp.

Bendat, J.S., Piersol, A.G., 1986. Random data. John Wiley & Sons, New York, New York.

Berquist, J. R., 1978. Depositional history and fault-related studies, Bolinas Lagoon, California. U. S. Geological Survey Open-file Report 78-802, 160 pp.

Bird, P., Kong, X., 1994. Computer simulations of California tectonics confirm very low strength of major faults. Geological Society America Bulletin 106, 159–174.

Bruns, T.R., Cooper, A.K., Carlson, P.R., McCulloch, D.S., 2002. Structure of the submerged San Andreas and San Gregorio fault zones in the Gulf of the Farallones as inferred from high-resolution seismic-reflection data. In: Parsons, T. (Ed.), Crustal Structure of the Coastal and Marine San Francisco Bay region, California. U. S. Geological Survey Professional Paper, pp. 77–117. 1658.

Burgmann, R., Segall, P., Lisowski, M., Svarc, J., 1997. Postseismic strain following the 1989 Loma Prieta earthquake from GPS and leveling measurements. Journal of Geophysical Research 102, 4933–4955.

Burgmann, R., Hilley, G., Ferretti, A., Novali, F., 2006. Resolving vertical tectonics in the San Francisco Bay area from scatterer InSAR and GPS analysis. Geology 34, 221–224.

California Geological Survey (CGS), 2006. Digital database of Quaternary and younger faults from the fault activity map of California. Version 2.0. http://www.consrv.ca.gov/CGS/information/publications/QuaternaryFaults_ver2.htm.

Childs, J.R., Hart, P.E., Sliter, R., Bruns, T.R., Marlow, M., 2000. High-resolution marine seismic reflection data from the San Francisco Bay area: 1993–1997. U. S. Geological Survey Open File Report 00-494.

Clifton, H.E., Hunter, R.E., 1987. The Merced Formation and related beds; a mile-thick succession of late Cenozoic coastal and shelf deposits in the seacliffs of San Francisco, CA. In: Hill, M.L. (Ed.), Cordilleran Section of the Geological Society of America Centennial Field Guide, Volume 1, pp. 257–262.

Clifton, H.E., Hunter, R.E., 1991. Depositional and other features of the Merced Formation in sea cliff exposures south of San Francisco, CA. In: Sloan, D., Wagner, D.L. (Eds.), Geologic Excursions in northern California: San Francisco to the Sierra Nevada. California Division of Mines and Geology Special Publication, 109, pp. 11–24.

Clifton, H.E., Hunter, R.E., Gardner, J.V., 1988. Analysis of eustatic tectonic and sedimentologic influences on transgressive and regressive cycles in the late Cenozoic Merced Formation, San Francisco, California. In: Paola, C., Kleinspehn, K.L. (Eds.), New Perspectives in Basin Analysis. Springer-Verlag, New York, pp. 109–128.

Cooper, A.K., 1973. Structure of the continental shelf west of San Francisco, California. U. S. Geological Survey Open-file Report 1907. 65 pp.

Dickinson, W.R., Ducea, M., Rosenberg, L.I., Greene, H.G., Graham, S.A., Clark, J.C., Weber, G.E., Kidder, S., Ernst, W.G., Brabb, E.E., 2005. Net dextral slip, Neogene San Gregorio–Hosgri fault zone, coastal California: geologic evidence and tectonic implications. Geological Society America Special Paper 391 43 pp.

Galloway, A.J., 1977. Geology of the Point Reyes Peninsula, Marin County, California. California Division of Mines and Geology Bulletin 202 72 pp.

Geist, E.L., Zoback, M.L., 1999. Analysis of the tsunami generated by the M_w 7.8 1906 San Francisco earthquake. Geology 27, 15–18.

Geist, E.L., Andrews, D.J., 2000. Slip rates on San Francisco Bay area faults from anelastic deformation of the continental lithosphere. Journal of Geophysical Research 105, 25543–25552.

Gerya, T.V., Yuen, D.A., 2007. Robust characteristics method for modelling multiphase visco-elasto-plastic thermo-mechanical problems. Physics Earth Planetary Interiors 163, 83–105.

Graymer, R.W., Sarna-Wojcicki, A.M., Walker, J.P., McLaughlin, R.J., Fleck, R.J., 2002. Controls on timing and amount of right-lateral offset on the East Bay fault system, San Francisco Bay region, California. Geological Society of America Bulletin 114, 1471–1479.

Grove, K., 2003. Coastal uplift of the Point Reyes Peninsula north of San Francisco. Geological Society of America 35 (4), 20 Abstr with Progr.

Grove, K., Niemi, T.M., 2005. Late Quaternary deformation and slip rates in the northern San Andreas fault zone at Olema Valley, Marin County, California. Tectonophysics 401, 231–250.

Hall, N.T., Wright, R.H., Clahan, K.B., 1999. Paleoseismic studies of the San Francisco Peninsula segment of the San Andreas fault zone near Woodside, California. Journal of Geophysical Research 104 (B10), 23215–23236.

Ingram, B.L., Ingle, J.C., 1998. Strontium isotope ages of the marine Merced Formation near San Francisco, California. Quaternary Research 50, 194–199.

Jachens, R.C., Zoback, M.L., 1999. The San Andreas fault in the San Francisco Bay region, California: Structure and kinematics of a young plate boundary. International Geology Review 41, 191–205.

Kennedy, D.G., , 2002. Neotectonic character of the Serra Fault, northern San Francisco Peninsula. California, M.S, thesis, San Francisco State University, Calif, 131 pp.

Kenner, S.J., Segall, P., 2000. Postseismic deformation following the 1906 San Francisco earthquake. Journal of Geophysical Research 105, 13195–13209.

Lachenbruch, A.H., Sass, J.H., 1980. Heat flow and energetics of the San Andreas fault zone. Journal of Geophysical Research 85, 6185–6222.

Lanphere, M.A., Champion, D.E., Clynne, M.A., Muffler, L.J.P., 1999. Revised age of the Rockland tephra, northern California: implications for climate and stratigraphic reconstructions in the western United States: Comment. Geology 27, 135–138.

Lawson, A.C., 1908. (Chairman) The California earthquake of April 18, 1906. Report of the State Earthquake Investigation Commission, vol. 1. Carnegie Institution of Washington Publication, Washington, D. C. 451 pp.

Lomax, A., 2005. A reanalysis of the hypocentral location and related observations for the Great 1906 California earthquake. Bulletin of the Seismological Society of America 95 (3), 861–877.

McCulloch, D.S., 1976. Acoustic reflection profiles, *R/V* KELEZ, April 1973 (Leg 1) Gulf of Farallones, central California offshore. U. S. Geological Survey Open File Report 76-736. 52pp.

McCulloch, D.S., 1987. Regional geology and hydrocarbon potential of offshore central California. In: Scholl, D.W., Grantz, A., Vedder, J.G. (Eds.), Geology and resource potential of the continental margin of western North America and adjacent ocean basins — Beaufort Sea to Baja California. Circum-Pacific Council for Energy and Mineral Resources, Houston, TX, pp. 353–401.

McLaughlin, R.J., Sliter, W.V., Sorg, D.H., Russell, P.C., Sarna-Wojcicki, A.M., 1996. Large-scale right-slip displacement on the East San Francisco Bay Region fault system, California: implications for location of late Miocene to Pliocene Pacific plate boundary. Tectonics 15, 1–18.

McLaughlin, R.J., Langenheim, V.E., Schmidt, K.M., Jachens, R.C., Stanley, R.G., Jayko, A.S., McDougall, K.A., Tinsley, J.C., Valin, Z.C., 1999. Neogene contraction between the San Andreas fault and the Santa Cara Valley, San Francisco Bay region, California. International Geology Review 41, 1–30.

McLaughlin, R. J., Powell, C. L., McDougal-Reid, K., and Jachens, R. C., 2007. Cessation of slip on the Pilarcitos Fault and initiation of the San Francisco Peninsula segment of the (modern) San Andreas Fault, California. Trans. AGU Fall Meeting, San Francisco.

Miller, S.A., 1996. Fluid-mediated influence of adjacent thrusting on the seismic cycle at Parkfield. Nature 382, 799–802.

Moresi, L., Dufour, F., Mühlhaus, H.B., 2003. A Lagrangian integration point finite element method for large deformation modeling of viscoelastic geomaterials. Journal Computational Physics 184, 476–497.

Muhlhaus, H.B., Regenauer-Lieb, K., 2005. Towards a self-consistent plate mantle model that includes elasticity: simple benchmarks and application to basic modes of convection. Geophysical Journal International 163, 788–800.

Niemi, T.M., Hall, N.T., 1992. Late Holocene slip rate and recurrence of great earthquakes on the San Andreas fault in northern California. Geology 20, 195–198.

Northern California earthquake data center (NCEDC), 2006. Data collections. http://www.ncedc.org/ncedc/.

NOAA 2001. Sea level variations of the United States 1854–1999. NOAA Technical Report NOS CO-OPS 36, Silver Spring, Maryland, 60 pp.

Parsons, T., 2002. Post-1906 stress recovery of the San Andreas fault system from 3-D finite element analysis. Journal of Geophysical Research 107. doi:10.1029/2001JB001051.

Parsons, T., 2006a. Tectonic stressing in California modeled from GPS observations. Journal of Geophysical Research 111. doi:10.1029/2005JB003946.

Parsons, T., 2006b. $M \geq 7.0$ earthquake recurrence on the San Andreas fault from a stress renewal model. Journal of Geophysical Research 111. doi:10.1029/2006JB004415.

Parsons, T., Zoback, M.L., 1997. Three-dimensional upper crustal velocity structure beneath San Francisco Peninsula, California. Journal of Geophysical Research 102 (B3), 5473–5490.

Parsons, T., Stein, R.S., Simpson, R.W., Reasenberg, P.A., 1999. Stress sensitivity of fault seismicity: a comparison between limited-offset oblique and major strike–slip faults. Journal of Geophysical Research 104, 20183–20202.

Parsons, T., Sliter, R., Geist, E.L., Jachens, R.C., Jaffe, B.E., Foxgrover, A., Hart, P.E., McCarthy, J., 2003. Structure and mechanics of the Hayward–Rodgers Creek fault stepover, San Francisco Bay, California. Bulletin of the Seismological Society of America 93, 2187–2200.

Powell II, C.L., Baron, J.A., Sarna-Wojcicki, A., Clark, J.C., Perry, F.A., Brabb, E.E., Fleck, R.J., 2007. Age, stratigraphy, and correlation of the Late Neogene Purisima Formation, central California Coast Ranges. U. S. Geological Survey Professional Paper 1740. 32pp.

Reasenberg, P.A., Simpson, R.W., 1992. Response of regional seismicity to the static stress change produced by the Loma Prieta earthquake. Science 255, 1687–1690.

Rogge, E. H., and LaForce, M. J., 2002. Hydrostratigraphy of the Westside Groundwater Basin, San Francisco and San Mateo Counties, California. Eos. Trans. AGU 83 (47), Fall Meet. Suppl., Abstract H52B-0684.

Ryan, H.F., Noble, M., 2002. Sea level response to ENSO along the central California coast: how the 1997–98 event compares with the historic record. Progress in Oceanography 54, 149–169.

Sarna-Wojcici, A.M., 2000. Revised age of the Rockland tephra, northern California: Implications for climate and stratigraphic reconstructions in the western United States: comment. Geology 28, 286.

Sarna-Wojcicki, A.M., Meyer, C.E., Bowman, H.R., Hall, N.T., Russell, P.C., Woodward, M.J., Slate, J.L., 1985. Correlation of the Rockland ash bed, a 400,000-year-old stratigraphic marker in northern California and western Nevada, and implications for middle Pleistocene paleogeography of central California. Quaternary Geology 23, 236–257.

Savage, J.C., Gan, W., Prescott, W.H., Svarc, J.L., 2004. Strain accumulation across the Coast Ranges at the latitude of San Francisco, 1994–2000. Journal of Geophysical Research 109 (B03413). doi:10.1029/2003JB002612.

Simpson, G.D., Thompson, S.C., Noller, J.S., Lettis, W.R., 1997. The northern San Gregorio fault zone: Evidence for the timing of late Holocene earthquakes near Seal Cove, California. Bulletin of the Seismological Society of America 87 (5), 1158–1170.

Sylvester, A.G., 1976. Tectonic transpression and basement-controlled deformation in San Andreas fault zone, Salton Trough, California. AAPG Bulletin 60, 2081–2102.

ten Brink, U.S., Driscoll, N.W., 1999. High-resolution images of the San Andreas fault offshore San Francisco. Eos Trans. AGU, 80(46), p. F707.

Author's personal copy

Thatcher, W., Marshall, G., Lisowski, M., 1997. Resolution of fault slip along the 470-km-long rupture of the great 1906 San Francisco earthquake and its implications. Journal of Geophysical Research 102, 5353–5367.

U. S. Geological Survey (USGS), 2006. NAMSS: National Archive of Marine Seismic Surveys. http://walrus.wr.usgs.gov/NAMSS/.

Working Group on California Earthquake Probabilities, 2003. Earthquake probabilities in the San Francisco Bay region: 2002 to 2031. U. S. Geological Survey Open-File Report 03-214.

Wakabayashi, J., Hengesh, J.V., Sawyer, T.L., 2004. Four-dimensional transform fault processes: progressive evolution of step-overs and bends. Tectonophysics 392, 279–301.

Zoback, M.D., 1991. State of stress and crustal deformation along weak transform faults. Philosophical Transactions of the Royal Society of London A337, 141–150.

Zoback, M.L., Jachens, R.C., Olson, J.A., 1999. Abrupt along-strike change in tectonic style: San Andreas fault zone, San Francisco Peninsula. Journal of Geophysical Research 104 (B5), 10719–10742.